

Article

Cooling Subgrade Effectiveness by L-Shaped Two-Phase Closed Thermosyphons with Different Inclination Angles and XPS Insulation Boards in Permafrost Regions

Yalong Zhou ¹, Xu Wang ^{1,2,3,*}, Chunxiang Guo ¹, Yuan Hu ¹, Fei He ¹, Deren Liu ^{1,2} and Daijun Jiang ^{1,2,3}¹ School of Civil Engineering, Lanzhou Jiaotong University, Lanzhou 730070, China² National and Provincial Joint Engineering Laboratory of Road & Bridge Disaster Prevention and Control, Lanzhou 730070, China³ Key Laboratory of Road & Bridge and Underground Engineering of Gansu Province, Lanzhou 730070, China

* Correspondence: publicwang@163.com

Abstract: This study focused on the coupling heat transfer mechanism and the cooling efficiency of L-shaped two-phase closed thermosyphons (L-shaped TPCTs) in the wide subgrade of permafrost regions. Considering the fact that time–space dynamics change the effects of the air temperature, wind speed, and geotemperature, a coupled air temperature–L-shaped TPCT–subgrade soil heat transfer model was established using the ANSYS 15.0 software platform, and the rationality of the model was verified through measured data. The heat-transfer characteristics of the L-shaped TPCTs and the long-term thermal stability of the subgrade were studied under different inclination angles of the evaporator ($\alpha = 15^\circ, 30^\circ, 50^\circ, 70^\circ$, and 90°). Then, the cooling effectiveness of a composite subgrade with TPCTs and an XPS insulation board was numerically calculated. The results show that the heat flux of the L-shaped TPCT was the greatest when $\alpha = 50^\circ$, and the heat flux reached the maximum value of $165.7 \text{ W}\cdot\text{m}^{-2}$ in January. The L-shaped TPCT had a relatively good cooling effect on the subgrade as a whole when $\alpha = 50^\circ$ and 70° , but the thawing depth at the center of the subgrade with L-shaped TPCTs reached 9.0 m below the ground surface in the 30th year. The composite subgrade with L-shaped TPCTs/vertical TPCT/XPS insulation board is an effective method to protect the permafrost foundation and improve the long-term thermal stability of the wide subgrade. The maximum heat flux of evaporation section of the L-shaped TPCT is 18.8% higher than that of the vertical TPCT during the working period of the TPCTs of the composite subgrade.

Keywords: permafrost; composite subgrade; L-shaped TPCT; XPS insulation board; coupled heat transfer model; cooling effectiveness



Citation: Zhou, Y.; Wang, X.; Guo, C.; Hu, Y.; He, F.; Liu, D.; Jiang, D. Cooling Subgrade Effectiveness by L-Shaped Two-Phase Closed Thermosyphons with Different Inclination Angles and XPS Insulation Boards in Permafrost Regions. *Materials* **2022**, *15*, 8470. <https://doi.org/10.3390/ma15238470>

Academic Editor: Miguel Ángel Sanjuán

Received: 23 October 2022

Accepted: 21 November 2022

Published: 28 November 2022

Publisher's Note: MDPI stays neutral with regard to jurisdictional claims in published maps and institutional affiliations.



Copyright: © 2022 by the authors. Licensee MDPI, Basel, Switzerland. This article is an open access article distributed under the terms and conditions of the Creative Commons Attribution (CC BY) license (<https://creativecommons.org/licenses/by/4.0/>).

1. Introduction

The Qinghai–Tibet Plateau is characterized by a low latitude, high altitude, and strong solar radiation; therefore, the proposed Qinghai–Tibet expressway crosses extensive permafrost regions [1–3]. The wide subgrade of the expressway has a large heat storage capacity. After its construction, the strong heat absorption of black asphalt pavement will lead to a “heat gathering effect” in the center of the subgrade, which will cause the permafrost below the subgrade to melt rapidly [3–5]. Therefore, under the influence of engineering activities and global warming, a technique for ground heat control to meet the demands of the long-term thermal stability of the subgrade is an important issue in the construction of expressways in permafrost regions.

The TPCT is a wickless heat transfer device with a highly efficient energy-transfer capacity, and it requires no external power supply. The XPS insulation board has low thermal conductivity, high compression resistance, and high aging resistance. The TPCT and XPS insulation board have been widely used in permafrost regions to ensure thermal stability,

such as the Qinghai–Tibet railway, Qinghai–Tibet highway, Qinghai–Tibet power transmission line, and China–Russia oil pipeline [6–12]. TPCTs are usually inserted vertically into a subgrade at the shoulders or toes along the subgrade direction in permafrost regions. The soil near the shoulder has a good cooling effect under this measure, but this cooling effect on the soil at the center of the subgrade is small [13,14]. In recent years, to expand the cooling range of the wide subgrade, effectively eliminate the “heat gathering effect” of the road substrate, and ensure the uniform and symmetrical distribution of the temperature field of the wide expressway subgrade in the permafrost regions, researchers have designed inclined or curved gravity TPCTs to expand the cooling range of the foundation [15–19].

The research results of Mozumder et al. [20], Sarmasti et al. [21], and Cao et al. [22] have shown that the flow state of the working medium inside the TPCT is extremely complex, and the heat transfer performance of the TPCT is affected by many factors, such as the geometric shape (diameter, length, and shape), working fluid, filling ratio, wall material, radiator surface area, and inclination angle. Zhang et al. [23] found that the total thermal resistance of the inclined TPCT is at a minimum when the inclination angle is 20° and a maximum when the inclination angle is 80° through indoor tests; Yang et al. [24] obtained that, when the inclination angle of the TPCT of the Qinghai–Tibet railway is 25°–30°, the lifting effect of the permafrost table at the center of subgrade, shoulder, and slope toe is the best. Pei et al. [25] studied the cooling effect of L-shaped TPCTs on the subgrade when the evaporator section is 45°. However, the cooling efficiency of the L-shaped TPCT in the permafrost subgrade is related not only to the design parameters of the TPCT and the inclination angles of the evaporator section, but also to the actual subgrade geometry and frozen soil environment. Therefore, it is necessary to study the coupling heat-transfer characteristics of L-shaped TPCTs in a wide subgrade under different inclination angles and its cooling effectiveness on subgrade soil, along with its influence on the long-term thermal stability of the wide subgrade with L-shaped TPCTs and the XPS insulation board.

From this perspective, this paper considers the time–space dynamic change effects of the air temperature, wind speed, and the geotemperature, establishing a coupled air temperature–L-shaped TPCT–subgrade soil heat transfer model. The different inclinations ($\alpha = 15^\circ, 30^\circ, 50^\circ, 70^\circ, \text{ and } 90^\circ$) of the evaporator section of L-shaped TPCTs and the geotemperature distribution of the subgrade are calculated and analyzed. The long-term thermal stability of the wide subgrade with the L-shaped TPCTs/vertical TPCT/XPS insulation board system in permafrost regions was evaluated.

2. Heat Transfer Model of the Subgrade with L-Shaped TPCTs

2.1. Heat Conduction Equation of Soil

Considering the heat conduction of the soil skeleton and water, along with the frozen soil phase change, the differential equation of heat conduction in the soil is as follows [26,27]:

$$\rho C \frac{\partial T}{\partial t} = \frac{\partial}{\partial x} \left(\lambda \frac{\partial T}{\partial x} \right) + \frac{\partial}{\partial y} \left(\lambda \frac{\partial T}{\partial y} \right) + \frac{\partial}{\partial z} \left(\lambda \frac{\partial T}{\partial z} \right), \quad (1)$$

where T is the soil temperature ($^\circ\text{C}$), ρ is the soil density ($\text{kg}\cdot\text{m}^{-3}$), λ is the thermal conductivity of soil ($\text{W}\cdot\text{m}^{-1}\cdot^\circ\text{C}^{-1}$), C is the specific heat capacity of the soil ($\text{J}\cdot\text{kg}^{-1}\cdot^\circ\text{C}^{-1}$), and t is the time (s).

The sensible heat capacity method is used to simulate the frozen soil phase change. Assuming that the soil phase-change temperature range is $(T_m \pm \Delta T)$, the simplified equivalent thermal conductivity and specific heat capacity can be expressed as

$$\lambda_e = \begin{cases} \lambda_f & T < T_m - \Delta T \\ \lambda_f + \frac{\lambda_u - \lambda_f}{2\Delta T} [T - (T_m - \Delta T)] & T_m - \Delta T \leq T \leq T_m + \Delta T \\ \lambda_u & T \geq T_m + \Delta T \end{cases}, \quad (2)$$

$$C_e = \begin{cases} C_f & T < T_m - \Delta T \\ \frac{L_s}{2\Delta T} + \frac{C_f + C_u}{2} & T_m - \Delta T \leq T \leq T_m + \Delta T \\ C_u & T \geq T_m + \Delta T \end{cases}, \quad (3)$$

where the subscripts f and u represent the frozen and unfrozen state of soil, respectively. C_e and λ_e are the equivalent thermal conductivity and specific heat capacity of soil, respectively. L_s is the latent heat of soil phase change.

2.2. Coupled Air Temperature—L-Shaped TPCT—Subgrade Soil Heat Transfer Model

Figure 1 shows the working mechanism diagram and thermal resistance network of an L-shaped TPCT. Ammonia is used as the working medium for the TPCT, and the starting temperature difference is 0.5 °C. The length of the condensation section (L_c) is 1.20 m, the length of the adiabatic section (L_a) is 0.80 m, and the length of the evaporator section (L_e) is 8.48 m. The inner diameter (d_i) and outer diameter (d_o) of the pipe are 0.057 m and 0.064 m, respectively. The fin height (b_n), the fin space (s_n), and the fin thickness (δ) are 0.025 m, 0.01 m, and 0.0015 m, respectively. The thermal conductivity coefficient of the pipe (λ) is $48 \text{ W}\cdot\text{m}^{-1}\cdot\text{C}^{-1}$.

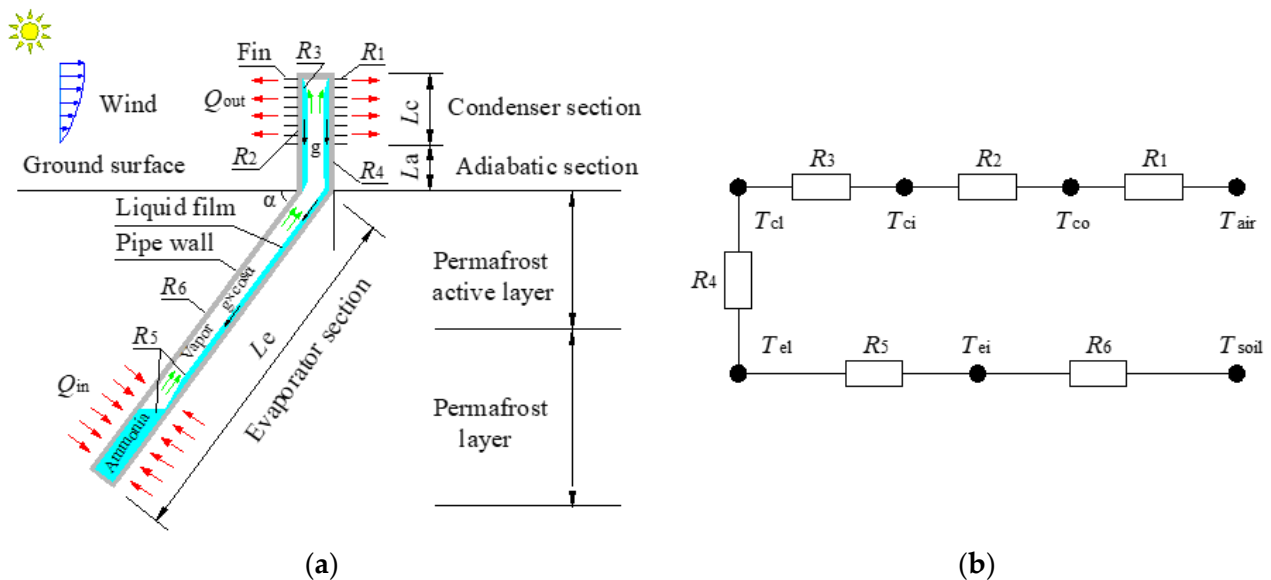


Figure 1. (a) Working mechanism diagram and (b) thermal resistance network of an L-shaped TPCT.

The equivalent thermal resistance of an L-shaped TPCT can be calculated using Equations (4)–(9) [25,28,29]. Table 1 shows the physical parameters of air [25], and Table 2 shows the physical parameters of the working medium of the TPCT [28,29]. n is the number of fins, and r_1 and r_2 are the outer diameters of the smooth pipe and fins, respectively. A_{c1} is the superficial area of the condenser section without fins, A_{c2} is the superficial area of the condenser section with fins, and A_{c3} is the total superficial area of the smooth condenser section. d_{co} and d_{ci} are the outer diameter and inner diameter of the condenser section, whereas d_{eo} and d_{ei} are the outer diameter and inner diameter of the evaporator section. V is the wind speed. η is the heat transfer efficiency of the fins. Re_a and Pr_a are the Reynolds number and Prandtl number of the flow through the outside surface of the condenser, respectively. λ_a , ρ_a , $c_{a,r}$ and ν are the thermal conductivity, density, specific heat at a constant pressure, and dynamic viscosity of air, respectively. ρ_l , λ_l , c_{pl} , L_x , μ , and ρ_{va} are the density, thermal conductivity, volumetric heat capacity, latent heat, dynamic viscosity, and density of the working medium, respectively. p_{sat} and p_a are the saturated and standard atmospheric pressure, respectively. g is the acceleration due to gravity. α is the angle of inclination between the evaporator section and the horizontal direction.

Table 1. Physical parameters of air [25].

Parameter	λ_a ($\text{W}\cdot\text{m}^{-1}\cdot\text{C}^{-1}$)	c_a ($\text{J}\cdot\text{kg}^{-1}\cdot\text{C}^{-1}$)	ρ_a ($\text{kg}\cdot\text{m}^{-3}$)	μ ($\text{Pa}\cdot\text{s}$)
Value	0.023	10040	0.641	1.75×10^{-5}

Table 2. Physical parameters of the working medium [29].

Parameter	λ_l ($\text{W}\cdot\text{m}^{-1}\cdot\text{C}^{-1}$)	c_{pa} ($\text{J}\cdot\text{kg}^{-1}\cdot\text{C}^{-1}$)	ρ_l ($\text{kg}\cdot\text{m}^{-3}$)	ρ_{va} ($\text{kg}\cdot\text{m}^{-3}$)	μ ($\text{Pa}\cdot\text{s}$)	L_r ($\text{kJ}\cdot\text{kg}^{-1}$)
Value	0.298	2125	638.6	3.48	2.35×10^{-4}	1263

The equivalent thermal resistance of an L-shaped TPCT can be calculated as follows:

(1) Condenser section

R_1 is the thermal resistance between the air and the outer wall of the condenser section [25,28]:

$$R_1 = \frac{1}{A_{c3}h_{co}}, \quad (4)$$

where $A_{c1} = \pi d_{co}(L_c - n\delta)$, $A_{c2} = \pi[2n(r_2^2 - r_1^2) + 2nr_2\delta]$, $A_{c3} = \pi d_{co}L_c$, $h_{co} = h_a \frac{A_{c1} + \eta A_{c2}}{A_{c3}}$, and $h_a = 0.1378 \frac{\lambda_a}{d_{co}} Re_a^{0.718} Pr_a^{\frac{1}{3}} \left(\frac{s_n}{b_n}\right)^{0.296}$.

R_2 is the thermal resistance for the tube wall of the condenser section [25,28]:

$$R_2 = \frac{1}{2\pi\lambda L_c} \ln(d_{co}/d_{ci}). \quad (5)$$

R_3 is the thermal resistance for the liquid film formed on the inner condenser section [25,28]:

$$R_3 = \frac{1}{A_{ci}h_{ci}}, \quad (6)$$

where $A_{ci} = \pi d_{ci}L_c$, and $h_{ci} = 0.925 \left(\frac{\lambda_l^3 \rho_l^2 g L_r}{\mu q_c L_c}\right)^{1/3}$.

(2) Adiabatic section

R_4 is the thermal resistance of the adiabatic section. When the TPCT is working, $R_4 = 0$. When the TPCT stops working, $R_4 = +\infty$.

(3) Evaporator section

R_5 is the thermal resistance for the liquid film and liquid pool in the evaporator [25,28]:

$$R_5 = \frac{1}{A_{ei}h_e}, \quad (7)$$

where $A_{ei} = \pi d_{ei}L_e$, and $h_e = 0.32 \left(\frac{\rho_l^{0.65} \lambda_l^{0.3} c_{pl}^{0.7} g^{0.2} q_e^{0.4}}{\rho_{va}^{0.25} L_r^{0.4} \mu^{0.1}}\right) \cdot \left(\frac{p_{sat}}{p_a}\right)^{0.3}$.

R_6 is the thermal resistance for the tube wall in the evaporator [25,28]:

$$R_6 = \frac{1}{2\pi\lambda L_e} \ln(d_{eo}/d_{ei}). \quad (8)$$

Combined with the above formulas, the total effective thermal resistance can be obtained using the following formula [25,28]:

$$\sum R_i = R_1 + R_2 + R_3 + R_4 + R_5 + R_6. \quad (9)$$

The heat transfer efficiency of a TPCT is known to be closely related to its inclination angle; the condensation section of an L-shaped TPCT is vertical, and its evaporator section is inclined. Considering the tilt effect of the evaporator section, we calculated the equivalent

heat transfer coefficient rate of the evaporator at different inclination angles on the basis of a prior research experiment [30,31], and the results are presented in Figure 2. This “equivalent heat transfer coefficient rate” is utilized for calculating the heat transfer coefficient of the L-shaped TPCT at different inclination angles.

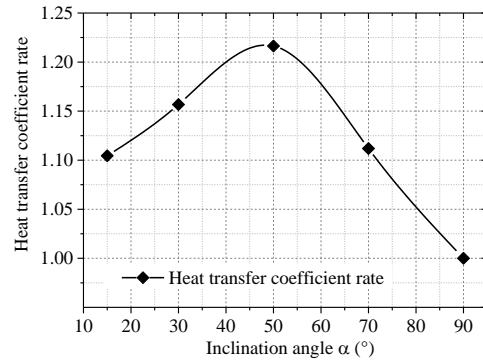


Figure 2. Heat transfer coefficient rate at different inclination angles of the evaporator.

Consequently, when the temperature difference between the evaporator and condenser section is greater than or equal to 0.5 °C, the total heat flow Q of an L-shaped TPCT is as follows [31,32]:

$$Q = \frac{T_a - T_{co}}{R_1} = \frac{T_{co} - T_{ci}}{R_2} = \frac{T_{ci} - T_{cl}}{R_3} = \frac{T_{cl} - T_{el}}{R_4} = \frac{T_{el} - T_{ei}}{R_5} = \frac{T_{ei} - T_s}{R_6} = \frac{T_a - T_s}{\sum R_i}, \tag{10}$$

where T_s is the soil temperature around the evaporator section, and T_a is the atmospheric temperature.

According to the heat balance theory, the heat absorbed by the evaporator section of the TPCT is equal to the heat lost by the condenser section when the heat loss is ignored. Therefore, the coupled air temperature–L-shaped TPCT–soil heat transfer model can be formalized as follows [31,32]:

$$\frac{T_s - T_a}{\pi d_o l_e \sum R_i} = \lambda_s \frac{\partial T}{\partial n}, \tag{11}$$

where λ_s is the thermal conductivity of soil.

3. Finite Element Calculation Model and Verification

3.1. Model Establishment and Boundary Conditions

On the basis of the meteorological conditions and engineering geological conditions in the permafrost regions of the Qinghai–Tibet Plateau, and referring to the relevant specifications for the design of high-grade highways in China [33], a finite element calculation model of subgrades for the wide high-grade highway with L-shaped TPCTs in permafrost regions was established using the ANSYS finite element software, as shown in Figure 3. In the model, part I is subgrade fill, part II is gravelly sand, part III is the clayey loam layer, and part IV is strongly weathered mudstone. The thermophysical parameters of different soils are shown in Table 3 [25].

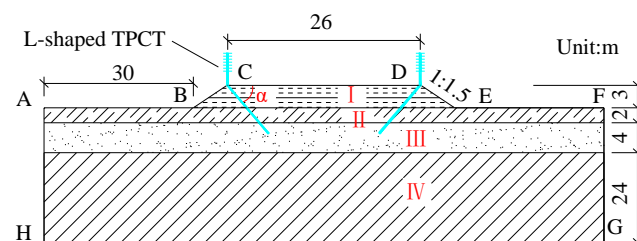


Figure 3. Calculation model of the subgrade with L-shaped TPCTs.

Table 3. Thermophysical parameters of different soils.

Soil Layer	Soil Layer Thickness (m)	Dry Density (kg·m ⁻³)	Thermal Conductivity (W·m ⁻¹ ·°C ⁻¹)		Specific Heat Capacity (J·kg ⁻¹ ·°C ⁻¹)		Latent Heat (J·m ⁻³)
			Frozen Soils	Unfrozen Soils	Frozen Soils	Unfrozen Soils	
Subgrade fill	3	2060	7128	6908	928	1081	2.04 × 10 ⁷
Gravelly sand	2	1900	5944	5220	960	1292	2.32 × 10 ⁷
Clayey loam	4	1600	4864	4050	1174	1473	6.03 × 10 ⁷
Mudstone	24	1800	6567	5306	1025	1166	3.77 × 10 ⁷

According to the observation data for the Qinghai–Tibet Plateau over many years, and considering the effects of global warming, the annual average air temperature will increase by about 2.6 °C in the coming 50 years. The temperature boundary conditions are simplified according to the boundary layer theory, and the simplified expressions of the temperature variations are given in Equation (6) and Table 4.

$$T_a = T_0 + A \sin\left(\frac{2\pi}{8760}t + \frac{\pi}{2} + \alpha_0\right) + \frac{2.6 \times t}{50 \times 365 \times 24}, \quad (12)$$

where T_0 is the mean annual ground temperature, A is the annual amplitude of temperature, t is the time in hours, and α_0 is the phase angle, which is determined by the finishing time of the subgrade.

Table 4. Temperature parameters of the upper surface [25].

Variable	T_0 (°C)	A (°C)
Air temperature	−3.0	10.5
Asphalt pavement surfaces (CD)	3.5	15
Slope surfaces (BC, DE)	1.7	13
Natural ground surfaces (AB, EF)	−0.5	12

According to the measured wind speed in the Qinghai–Tibet Plateau, the wind speed at the height H above the ground can be calculated using the following formula [28]:

$$V = (3.64 + 1.10 \sin(\frac{2\pi}{8760}t + \frac{3\pi}{2} + \alpha_0)) \left(\frac{H}{10}\right)^{0.16}, \quad (13)$$

where t is the time in hours, H is the height above the ground (m), and α_0 is the phase angle.

The left and right boundaries (AH and FG) of the computational model are assumed to be adiabatic, and a constant heat flux of $q = 0.03 \text{ W}\cdot\text{m}^{-2}$ is applied to the bottom boundary (HG) of the computational model. The heat flux of the evaporator section of the TPCT is applied to the model node in the form of linear heat flux.

In this study, we assumed that the subgrade was constructed on July 15 ($\alpha_0 = 0$). The initial temperature distributions of the natural foundation were obtained through a long-term transient solution with the boundary condition without considering global warming. Furthermore, it was found that the initial temperatures of the subgrade are dependent on the actual temperature of the natural ground surface. The APDL language in ANSYS was used to compile corresponding programs to realize the calculation of the coupled air temperature–L-shaped TPCT–subgrade soil heat transfer model.

3.2. Model Validation

In permafrost regions, the L-shaped TPCT has not been tested in the subgrade of a wide expressway, and there is still a lack of field data to verify the established model. However, the coupled model of a wide subgrade with an L-shaped TPCT established above is universal and can simulate various working conditions through changes in the boundary conditions, geological conditions, and model size. Pei et al. [25] carried out a field test on a subgrade with an L-shaped TPCT ($\alpha = 45^\circ$) in Bailu River, Qinghai–Tibet Plateau of China; the geological conditions of the test site, the geometric dimensions of the

subgrade, the frozen soil environment, and the L-shaped TPCT parameters were detailed in a previous study [25]. On the basis of field tests, the coupled model of the subgrade with L-shaped TPCTs was established using the ANSYS software, where the thermophysical and mechanical parameters of soil and the boundary conditions of the model were selected according to the numerical calculations found in previous literature [25]. To verify the rationality of the aforementioned models and calculation results, the calculated values of heat flux at the outer walls of the evaporator sections and the ground temperature at the centerline of the subgrade were selected and compared with the field-measured values, as shown in Figure 4.

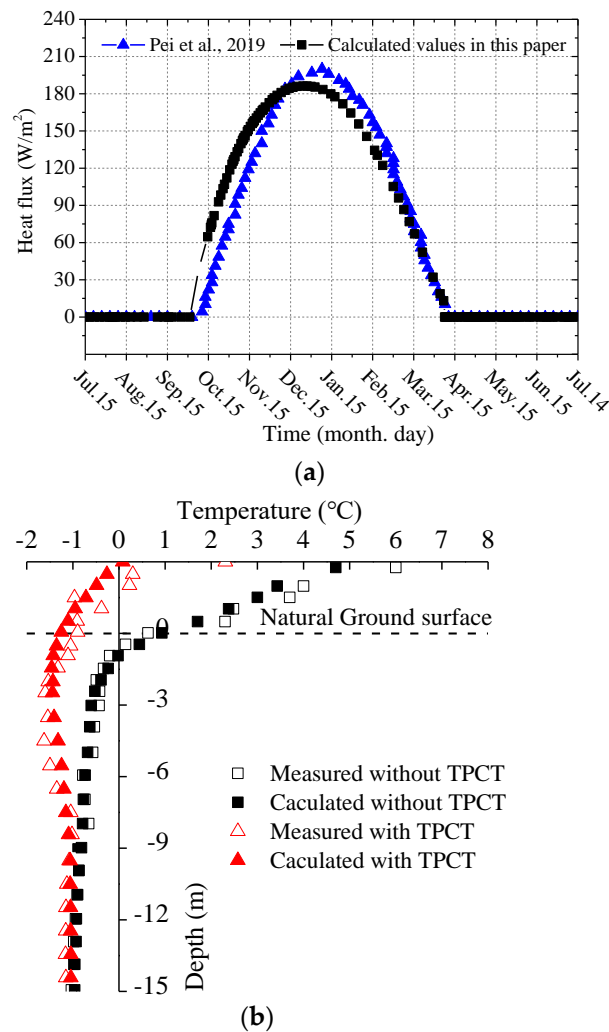


Figure 4. Validation of the numerical calculation results: (a) heat flux of the TPCT (fifth year) [25]; (b) geotemperatures at the of subgrade center (15 October, fifth year).

Figure 4a shows the comparison curves between the heat flux calculated by Pei et al. [26] and the value calculated in this paper. It can be seen from the figure that the change trend of the two curves remained basically consistent. The calculation results of the working start time, the working end time, and the change in the heat flux with time during the working period of the L-shaped TPCT in this paper are in good agreement with the findings of Pei et al. [25]. Figure 4b shows the comparison curves of the measured and calculated ground temperature at the subgrade center. It can be seen from the figure that the numerical simulation value of the ground temperature along the depth of the subgrade was basically consistent with the measured value. Only the surface near the subgrade had a relatively large error, which may have been due to the influence of ambient temperature, light, and other factors. On the basis of the heat-transfer characteristics of the L-shaped

TPCT and the comparison of the ground temperature of the subgrade, it can be concluded that the coupled heat transfer model can better predict the long-term thermal stability of the subgrade with L-shaped TPCTs in permafrost regions.

4. Influence of Evaporator Section Inclinations on the Cooling Effectiveness

The calculation models of an ordinary subgrade (no TPCT) and five wide subgrades with L-shaped TPCTs ($\alpha = 15^\circ, 30^\circ, 50^\circ, 70^\circ$, and 90°) were established. The heat-transfer characteristics of L-shaped TPCTs with different inclinations and the long-term thermal stability were analyzed.

4.1. Heat-Transfer Characteristics of L-Shaped TPCTs

Figure 5 shows the variations of the average temperatures at the outer walls of the evaporator sections of L-shaped TPCTs ($\alpha = 50^\circ$) with time. It can be seen that the temperature is closely related to the air temperature. When the atmospheric temperature is lower than the temperature at the outer walls of the evaporator sections, the L-shaped TPCTs begin to work. With decreases in the air temperature, the cooling performance of the L-shaped TPCTs is improved, and the temperature of the soil around evaporator sections decrease. In the warm season, the L-shaped TPCTs stop working and the temperature of soil around the evaporator sections increase. During the first 5 years, the temperatures at the outer walls of the evaporator sections decrease year by year, reaching a dynamic balance with the ground temperature of the surrounding soil in the fifth year. Then, with increases in the air temperature, it slowly increases.

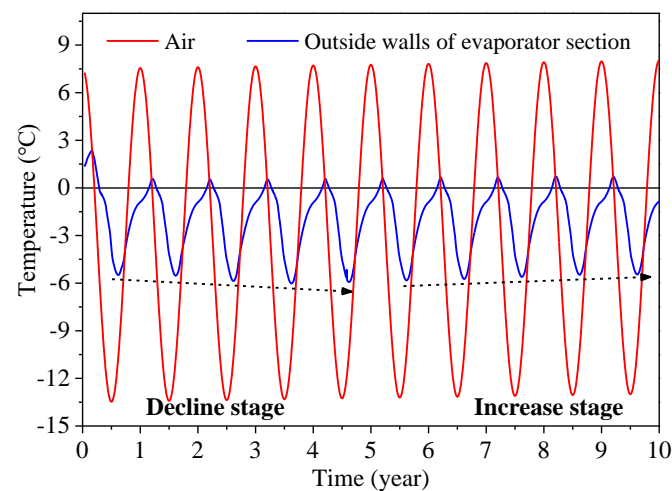


Figure 5. Variations in the average temperatures at the outer walls of the evaporator sections of L-shaped TPCTs with time ($\alpha = 50^\circ$).

Figure 6 shows the variations of the heat flux at the outer walls of the evaporator sections of L-shaped TPCTs during the fifth year. It can be seen from Figures 5 and 6 that the changes in the heat flux are closely related to the changes in the atmospheric temperature and the outer wall temperatures of the L-shaped TPCT evaporator sections. With decreases in the air temperature, the L-shaped TPCT begins to work, and the heat flux gradually increases. With increases in the air temperature, the heat flux decreases gradually until the L-shaped TPCT stops working. The heat flux is the largest when the inclination of the L-shaped TPCT evaporator section is 50° , reaching the maximum value of $165.7 \text{ W}\cdot\text{m}^{-2}$ in January. It can also be seen from the figure that the working hours of L-shaped TPCT with different inclinations are also different; a smaller inclination leads to longer working hours.

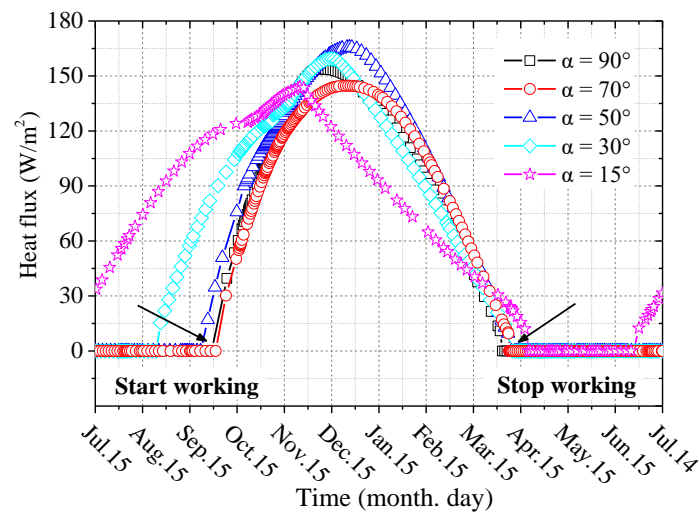


Figure 6. Variations in the heat flux at the outer walls of the evaporator sections of L-shaped TPCTs during the fifth year.

4.2. Geotemperature Distribution in the Subgrade

Figure 7 shows the geotemperature distributions in the subgrade without a TPCT on 1 October of the 30th year after construction. According to the calculation, the permafrost table of natural frozen soil before subgrade construction was 2.86 m. It can be seen from the figure that, within 30 years after the subgrade construction, the permafrost table ($0\text{ }^{\circ}\text{C}$ isotherm) at the shoulder decreased from 2.86 m below the ground surface to 11.7 m, and the permafrost table at the center of the subgrade decreased from 2.86 m below the ground surface to 14.37 m, forming a large melting circle for the entire subgrade. Therefore, the wide pavement of the expressway has a strong heat absorption capacity, which leads to the degradation of permafrost, particularly the severe degradation of permafrost at the center of the subgrade.

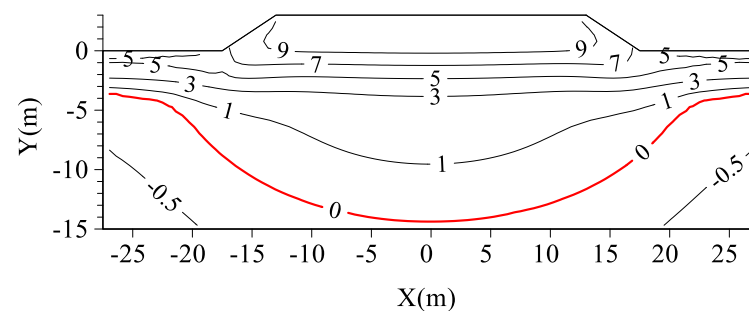


Figure 7. Geotemperature distributions of subgrades without a TPCT on 1 October of the 30th year after construction (Unit: $^{\circ}\text{C}$).

Figure 8 shows the geotemperature distributions of subgrades with L-shaped TPCTs under different α values on 1 October of the 30th year after their construction. In comparison to the geotemperature distributions of subgrades without TPCT (Figure 7), the melting circle of the subgrades with L-shaped TPCTs is obviously smaller. It can be seen that the inclination angle of the evaporator section has a great impact on the distribution of the temperature fields of the subgrades. The vertically placed TPCT (Figure 8e) has a good cooling effect on the soil at the shoulder, but has little impact on the temperature at the center of the subgrade.

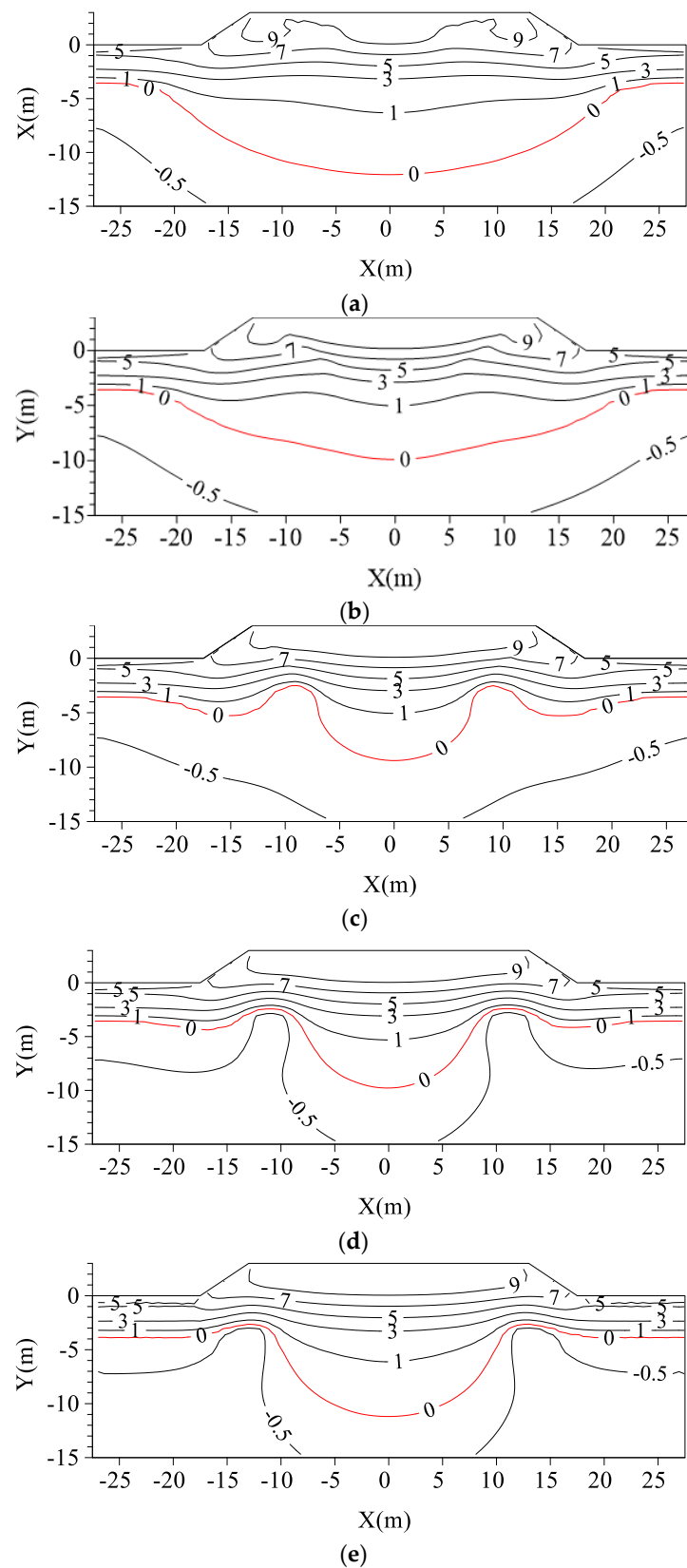


Figure 8. Geotemperature distributions of subgrades with L-shaped TPCTs under different α values on 1 October of the fifth year after their construction (unit: $^\circ\text{C}$): (a) $\alpha = 15^\circ$; (b) $\alpha = 30^\circ$; (c) $\alpha = 50^\circ$; (d) $\alpha = 70^\circ$; (e) $\alpha = 90^\circ$.

Figure 9 shows the thawing depth at the subgrade shoulder and center 30 years after subgrade construction. It can be seen that, when the inclination angles of the evaporator section are 50° and 70° , the thawing depth at the center of the subgrade is relatively small, and the melting depth is 9.39 m and 9.79 m below the natural ground surface, respectively.

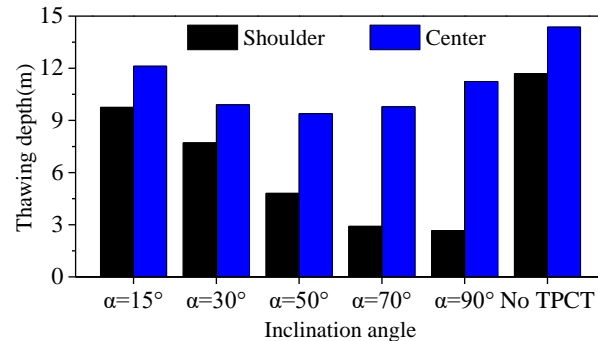


Figure 9. The thawing depth at the subgrade shoulder and center on 1 October after 30 years of construction.

In combination with Figure 6, Figure 8, and Figure 9, considering the heat transfer efficiency of the L-shaped TPCT, the geotemperature distributions of the subgrade, and the thawing depth at the shoulder and center of the subgrade, it can be concluded that the L-shaped TPCTs have relatively good cooling effects on the subgrade as a whole when the inclination angles of the evaporator section are 50° and 70° . However, in the 30th year, the thawing depth at the center of the subgrade with L-shaped TPCTs reaches 9 m below the ground surface; therefore, the L-shaped TPCT cannot be directly applied to the subgrade of a wide expressway alone. It also needs to be used in combination with other thermal insulation measures to ensure the long-term thermal stability of the subgrade.

5. Composite Subgrades with an L-Shaped TPCTs/Vertical TPCT/XPS Insulation Board System

XPS insulation boards are often used as engineering measures to control the ground temperature of frozen foundations, and they can prevent the heat of the asphalt pavement entering the frozen soil foundation during the warm season [34–36]. In order to further expand the cooling range and enhance the thermal stability of the wide subgrade, a TPCT is vertically buried at the central reservation of the expressway. The L-shaped TPCTs, vertical TPCT, and XPS insulation board are combined to form a composite subgrade structure. The length of the evaporator section of the vertical TPCT is 6.5 m, and other parameters are the same as the L-shaped TPCTs. XPS insulation boards are set at 1.0 m below the subgrade surface, with a lateral laying width of 29.0 m, as shown in Figure 10. The thickness of the XPS insulation board is 0.10 m, the density is $60 \text{ kg}\cdot\text{m}^{-3}$, the thermal conductivity is $0.03 \text{ W}\cdot\text{m}^{-1}\cdot^\circ\text{C}^{-1}$, the specific heat capacity is $140 \text{ J}\cdot\text{kg}^{-1}\cdot^\circ\text{C}^{-1}$, and other calculation parameters and boundary conditions are the same as those in Figure 3. Figure 11 shows the geotemperature distributions of the composite subgrade on 1 October of the 30th year after their construction.

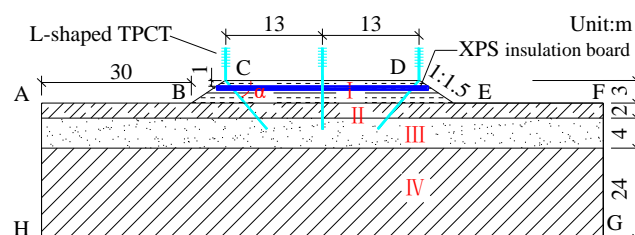


Figure 10. Calculation model of the composite subgrade.

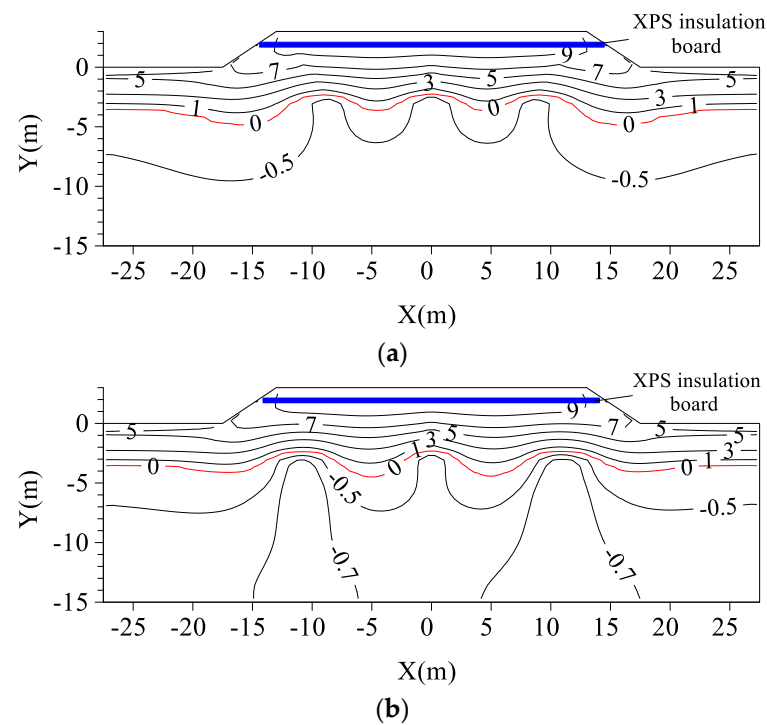


Figure 11. Geotemperature distributions of the composite subgrade on 1 October of the 30th year after their construction (Unit: °C): (a) $\alpha = 50^\circ$; (b) $\alpha = 70^\circ$.

It can be seen from Figure 11 that the composite subgrade increases the permafrost table at the center of the subgrade compared with the geotemperature distributions of the subgrade with L-shaped TPCTs (Figure 8c,d). The permafrost table of natural frozen soil in the 30th year is 3.53 m below the natural ground surface. When α is 50° and 70° , the permafrost table at the center of the composite subgrade is located at 3.64 m and 4.49 m below the natural ground surface, respectively. Therefore, the cooling effect of the composite subgrade is better when α is 50° , and the permafrost table at the center of the composite subgrade is 0.11 m lower than the permafrost table of the natural frozen soil at this time. It can be seen that the composite subgrade with the L-shaped TPCTs/vertical TPCT/XPS insulation board system has a good cooling effect, can resist the warming effect of the climate, and meet the long-term thermal stability requirements of the subgrade in permafrost regions.

Figure 12 shows the comparison curves of the heat flux at the outer wall of the evaporation section of the vertical TPCT and L-shaped TPCT (α is 50°). It can be seen from the figure that the startup time of L-shaped TPCT lags behind, and the corresponding end time also lags behind, where $\Delta t_1 = 12$ days and $\Delta t_2 = 7$ days. During the initial working period of TPCTs, the heat flux of the vertical TPCT of the composite subgrade is slightly higher than that of the L-shaped TPCT. After about 1 month, the heat flux of L-shaped TPCT is greater than that of vertical TPCT. The maximum heat flux of the L-shaped TPCT and the vertical TPCT is $196.8 \text{ W}\cdot\text{m}^2$ and $165.7 \text{ W}\cdot\text{m}^2$, respectively, throughout the working time, and the maximum heat flux of the L-shaped TPCT is 18.8% higher than that of the vertical TPCT. The main reasons for the above phenomena are the different lengths, inclinations, and positions of the evaporation section of TPCTs in the subgrade. In addition, the XPS insulation board exhibits a bidirectional heat resistance effect, which hinders the exchange of heat and cold energy between the atmospheric environment and the subgrade, leading to changes in the temperature difference between the outer wall of the evaporator section of the L-shaped TPCT and the atmospheric temperature, thus affecting the working state of the TPCTs.

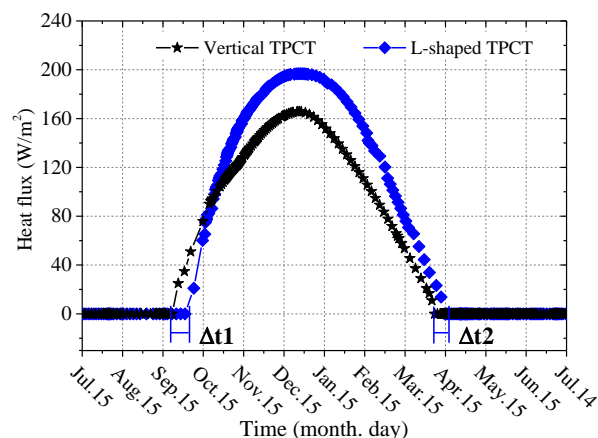


Figure 12. Comparison curves of the heat flux of the vertical TPCT and L-shaped TPCT of the composite subgrade.

6. Conclusions

In this paper, a coupled heat transfer model of air temperature–L-shaped TPCT–subgrade was established. The influence of the inclination angles of the evaporator section on the heat-transfer characteristics of the wide subgrade with an L-shaped TPCT in permafrost regions and the thermal stability of the subgrade 30 years later were simulated. The cooling effectiveness of the wide subgrade with L-shaped TPCTs/vertical TPCT/XPS insulation board system was calculated. The main conclusions are as follows:

1. A coupled heat transfer calculation model of air temperature–L-shaped TPCT–subgrade soil, considering the changes in the evaporator section inclination angles of the L-shaped TPCT, was proposed. The comparison between the calculated results and the field-measured data showed that the model could simulate the thermal stability of a wide subgrade with L-shaped TPCTs in permafrost regions.
2. In comparison to a vertical TPCT, the L-shaped TPCT had a relatively good cooling effect on the subgrade, as a whole, when the inclination angles of the evaporator section were 50° and 70° . However, in the 30th year, the thawing depth at the center of the subgrade with L-shaped TPCTs reached 9.0 m below the ground surface. When the evaporator section inclination angle of the TPCT was 50° , the corresponding heat flux was the largest, reaching a maximum value of $165.7 \text{ W}\cdot\text{m}^{-2}$ in January.
3. The composite subgrade with L-Shaped TPCTs/vertical TPCT/XPS insulation board system is an effective method to protect the permafrost foundation and improve the long-term thermal stability of a wide subgrade. The maximum heat flux of evaporation section of the L-shaped TPCT and vertical TPCT of the composite subgrade was $196.8 \text{ W}\cdot\text{m}^{-2}$ and $165.7 \text{ W}\cdot\text{m}^{-2}$, respectively, throughout the working time, and the maximum heat flux of L-shaped TPCT was increased by 18.8%. However, this paper only studied the influence of L-shaped two-phase closed thermosyphons and XPS insulation boards on the subgrade temperature field, and more studies should be carried out on the deformation of the composite subgrade in the future.

Author Contributions: Y.Z., conceptualization, methodology, formal analysis, and writing—original draft; X.W., project administration, resources, and funding acquisition; C.G., methodology and writing—review and editing; Y.H., data curation and visualization; F.H., data curation and writing—review & editing; D.L., methodology and resources; D.J., resources and supervision. All authors have read and agreed to the published version of the manuscript.

Funding: The research was funded by the National Natural Science Foundation of China (Grant No.41902272) and the Natural Science Foundation of Gansu Province, China (Grant No.20JR10RA235).

Institutional Review Board Statement: Not applicable.

Informed Consent Statement: Not applicable.

Data Availability Statement: Not applicable.

Acknowledgments: The authors appreciate the National Natural Science Foundation of China (Grant No. 41902272) and the Natural Science Foundation of Gansu Province, China (Grant No. 20JR10RA235).

Conflicts of Interest: The authors declare no conflict of interest.

References

1. Yu, Q.; Fan, K.; Qian, J.; Guo, L.; You, Y. Key issues of highway construction in permafrost regions in China. *Sci. Sin. Technol.* **2014**, *44*, 425–432.
2. Niu, F.; Luo, J.; Lin, Z.; Fang, J.; Liu, M. Thaw-induced slope failures and stability analyses in permafrost regions of the Qinghai-Tibet Plateau, China. *Landslides* **2016**, *13*, 55–65. [[CrossRef](#)]
3. Yu, F.; Qi, J.L.; Lai, Y.M.; Sivasithamparam, N.; Yao, X.L.; Zhang, M.Y.; Liu, Y.Z.; Wu, G.L. Typical embankment settlement/heave patterns of the Qinghai-Tibet highway in permafrost regions: Formation and evolution. *Eng. Geol.* **2016**, *214*, 147–156. [[CrossRef](#)]
4. Ma, W.; Mu, Y.H.; Xie, S.B.; Mao, Y.C.; Chen, D. Thermal-mechanical influences and environmental effects of expressway construction on the Qinghai-Tibet permafrost engineering corridor. *Adv. Earth Sci.* **2017**, *32*, 459–464.
5. Zhu, D.; Dong, Y.; Liu, G. Study of the influence of large-width asphalt-concrete pavement on the thermal characteristics of underlying permafrost. *J. Glaciol. Geocryol.* **2014**, *36*, 845–853.
6. Wu, Z.W.; Liu, Y.Z. *Frozen Subsoil and Engineering*; Ocean Press: Beijing, China, 2005.
7. Kong, S.; Wen, Z.; Wu, Q.; Wang, D. Applicability evaluation on application of thermosyphon in embankment engineering of expressway in permafrost regions of Qinghai-Tibet plateau. *J. Cent. South Univ. (Sci. Technol.)* **2019**, *50*, 1384–1391.
8. Wen, Z.; Sheng, Y.; Ma, W.; Qi, J. In situ experimental study on thermal protection effects of the insulation method on warm permafrost. *Cold Reg. Sci. Technol.* **2008**, *53*, 369–381. [[CrossRef](#)]
9. Heuer, C.E. *The Application of Heat Pipes on the Trans-Alaska Pipeline, United States Army Corps of Engineers*; Cold Regions Research and Engineering Laboratory: New Hampshire, NH, USA, 1979.
10. Ma, L.; Shang, L.; Zhong, D.; Ji, Z. Experimental investigation of a two-phase closed thermosyphon charged with hydrocarbon and Freon refrigerants. *Appl. Energy* **2017**, *207*, 665–673. [[CrossRef](#)]
11. Gao, J.; Lai, Y.; Zhang, M.; Chang, D. Thermal effect of heating two-phase closed thermosyphons on the high-speed railway embankment in seasonally frozen regions. *Appl. Therm. Eng.* **2018**, *141*, 948–957. [[CrossRef](#)]
12. Jiang, D.; Wang, X.; Liu, D.; Qiong, X. Experimental study on stability of thermal pile foundation of transmission tower in permafrost foundation of Qinghai-Tibet railway. *Chin. J. Rock Mech. Eng.* **2014**, *33*, 4258–4263.
13. Song, Y.; Jin, L.; Zhang, J. In-situ study on cooling characteristics of two-phase closed thermosyphon embankment of Qinghai-Tibet Highway in permafrost regions. *Cold Reg. Sci. Technol.* **2013**, *93*, 12–19. [[CrossRef](#)]
14. Yu, F.; Zhang, M.; Lai, Y.; Liu, Y.; Qi, J.; Yao, X. formation of a highway embankment installed with two-phase closed thermosyphons in permafrost regions: Field experiment and geothermal modelling. *Appl. Therm. Eng.* **2017**, *115*, 670–681. [[CrossRef](#)]
15. Dong, Y.H.; Lai, Y.M.; Chen, W. Cooling effect of combined L-shaped thermosyphon, crushed-rock revetment and insulation for high-grade highways in permafrost regions. *Chin. J. Geotech. Eng.* **2012**, *34*, 1043–1049.
16. Zhang, M.; Lai, Y.; Zhang, J.; Sun, Z. Numerical study on cooling characteristics of two-phase closed thermosyphon embankment in permafrost regions. *Cold Reg. Sci. Technol.* **2011**, *65*, 203–210. [[CrossRef](#)]
17. Zhang, M.Y.; Pei, W.S.; Lai, Y.M.; Niu, F.J.; Li, S.Y. Numerical study of the thermal characteristics of a shallow tunnel section with a two-phase closed thermosyphon group in a permafrost region under climate warming. *Int. J. Heat Mass Tran.* **2017**, *104*, 952–963. [[CrossRef](#)]
18. Wu, J.J.; Ma, W.; Sun, Z.Z.; Wen, Z. In-situ study on cooling effect of the two-phase closed thermosyphon and insulation combinational embankment of the Qinghai-Tibet Railway. *Cold Reg. Sci. Technol.* **2010**, *60*, 234–244. [[CrossRef](#)]
19. Zhang, M.; Lai, Y.; Wu, Q.; Yu, Q.; Zhao, T.; Pei, W.; Zhang, J. A full-scale field experiment to evaluate the cooling performance of a novel composite embankment in permafrost regions. *Int. J. Heat Mass Transf.* **2016**, *95*, 1047–1056. [[CrossRef](#)]
20. Mozumder, A.K.; Akon, A.F.; Chowdhury, M.S.H.; Banik, S.C. Performance of heat pipe for different working fluids and fill ratios. *J. Mech. Eng.* **2010**, *41*, 96–102. [[CrossRef](#)]
21. Eami, M.R.S.; Noie, S.H.; Khoshnoodi, M. Effect of aspect ratio and filling ratio on thermal performance of an tilted two-phase closed thermosyphon. *Iran. J. Sci. Technol. Trans. B Eng.* **2008**, *32*, 39–51.
22. Cao, X.L.; Cao, S.J.; Zhu, X.J.; Zeng, W.; Wang, F.F.; Li, J.; Chi, D. Experimental investigation on heat transfer characteristics of novel gravity-assisted heat pipe heat exchanger. *J. Cent. South Univ. (Sci. Technol.)* **2012**, *43*, 402–406.
23. Zhang, M.; Lai, Y.; Dong, Y.; Jin, L.; Pei, W.; Harbor, J. Laboratory investigation of the heat transfer characteristics of a two-phase closed thermosyphon. *Cold Reg. Sci. Technol.* **2013**, *95*, 67–73. [[CrossRef](#)]
24. Yang, Y.; Zhou, S.; Wei, Q. Effect simulation of different declining angles of thermosyphons used in Qinghai-Tibet railway permafrost embankment. *China Civ. Eng. J.* **2006**, *39*, 108–113.
25. Pei, W.; Zhang, M.; Lai, Y.; Yan, Z.; Li, S. Evaluation of the ground heat control capacity of a novel Air-L-Shaped TPCT-Ground (ALTG) cooling system in cold regions. *Energy* **2019**, *179*, 655–668. [[CrossRef](#)]

26. Zhou, Y.; Guo, C.; Wang, X.; Jiang, D.; Liu, D.; He, F.; Hu, Y. Prediction of long-term cooling effect of thermal pipe foundation of transmission tower in permafrost regions considering the change of thermal pipe power. *Chin. J. Rock Mech. Eng.* **2019**, *38*, 1461–1469.
27. Zhou, Y.; Wang, X.; Niu, F.; He, F.; Guo, C.; Liu, D.; Jiang, D. Frost jacking characteristics of transmission tower pile foundations with and without thermosyphons in permafrost regions of Qinghai–Tibet plateau. *J. Cold Reg. Eng.* **2021**, *35*, 04021004. [[CrossRef](#)]
28. Hou, Y.; Wu, Q.; Dong, J.; Luo, J.; Zhang, M.; Ye, Z. Numerical simulation of efficient cooling by coupled RR and TCPT on railway embankments in permafrost regions. *Appl. Therm. Eng.* **2018**, *133*, 351–360. [[CrossRef](#)]
29. Mu, Y.; Yu, Q.; Li, G.; Wei, M.; Mao, Y.-C.; Guo, L. Application of thermosyphons and insulated boards in Qinghai-Tibet DC interconnection project in permafrost regions. *Chin. J. Geotech. Eng.* **2014**, *36*, 1896–1907.
30. Fan, X. Study on heat transfer characteristics of gravity heat pipe and ground source heat pump composite rode snowmelt system. Master’s Thesis, Harbin Institute of Technology, Harbin, China, 2017.
31. Khazaee, I.; Hosseini, R.; Kianifar, A.; Noie, S.H. Experimental consideration and correlation of heat transfer of a two-phase closed thermosyphon due to the inclination angle, filling ratio, and aspect ratio. *J. Enhanc. Heat Transf.* **2011**, *18*, 31–40. [[CrossRef](#)]
32. Jin, L.; Wang, S.; Mu, k.; Hui, P. Cooling effect of thermosyphon subgrade for Qinghai-Tibet highway. *J. Traffic Transp. Eng.* **2016**, *16*, 45–58.
33. *JTG 3363–2019*; Code for Design of Ground Base and Foundation of Highway Bridges and Culverts. China Communications Press: Beijing, China, 2019.
34. She, W.; Chen, Y.Q.; Zhang, Y.S.; Jones, M.R. Characterization and simulation of microstructure and thermal properties of foamed concrete. *Constr. Build. Mater.* **2013**, *47*, 1278–1291.
35. Chen, D. Dynamic three-dimensional heat transfer calculation for uninsulated slab-on-ground constructions. *Energy Build.* **2013**, *60*, 420–428. [[CrossRef](#)]
36. Plotnikov, A. Stabilizing the temperature regime of a frozen foundation bed using thermal insulation and cooling mechanisms. *Soil Mech. Found. Eng.* **2020**, *57*, 329–335. [[CrossRef](#)]